iScience

CellPress
OPEN ACCESS

Article

TGF-β1 promotes osteogenesis of mesenchymal stem cells via integrin mediated mechanical positive autoregulation

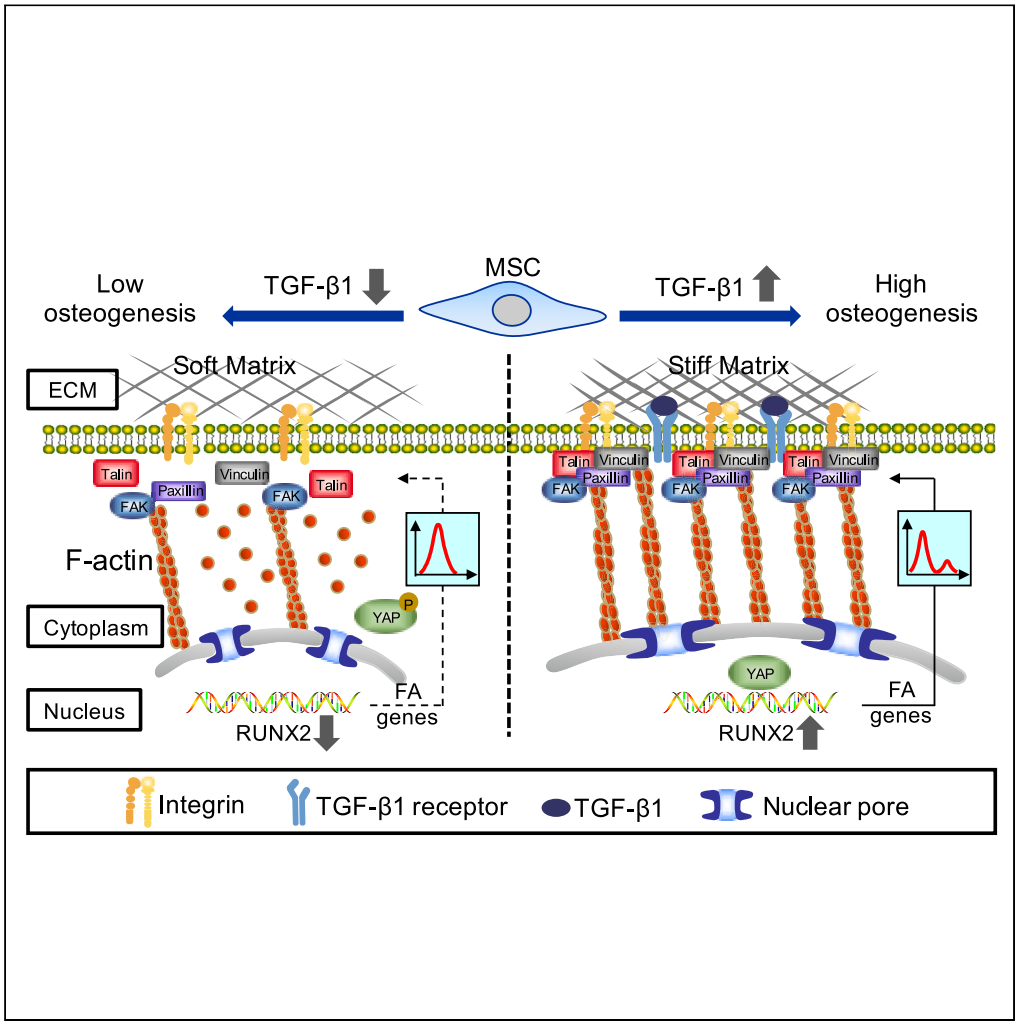

Wanting Wan, Hui Zhang, Lin Niu, ..., Dandan Pei, Min Lin, Bo Cheng

peidandan@xjtu.edu.cn (D.P.)
minlin@xjtu.edu.cn (M.L.)
chenbo8874@xjtu.edu.cn (B.C.)

Highlights

TGF-β1 promotes MSCs osteogenic differentiation by activating biophysical signaling

TGF-β1 induces the formation of PAR involving the integrin-FAK-YAP axis in MSCs

The feedback of mechanical PAR induces the bimodal distribution of focal adhesion

Wan et al., iScience 27, 110262
July 19, 2024
https://doi.org/10.1016/j.isci.2024.110262

iScience

CellPress
OPEN ACCESS

Article

TGF-β1 promotes osteogenesis of mesenchymal stem cells via integrin mediated mechanical positive autoregulation

Wanting Wan,[1,3] Hui Zhang,[1,3] Lin Niu,[1] Min Zhang,[4] Feng Xu,[2,3] Ang Li,[1] Dandan Pei,[1,*] Min Lin,[2,3,*] and Bo Cheng[2,3,5,*]

SUMMARY

Positive autoregulation (PAR), one type of network motifs, provides a high phenotypic heterogeneity for cells to better adapt to their microenvironments. Typical mechanosensitive proteins can also form PAR, e.g., integrin mediated PAR, but the role of such mechanical PAR in physiological development and pathological process remains elusive. In this study, we found that transforming growth factor β1 (TGF-β1) and integrin levels decrease with tissue softening after the development of paradentium *in vivo* in rat model of periodontitis (an inflammatory disease with bone defect). Interestingly, TGF-β1 could induce the formation of mechanical PAR involving the integrin-FAK-YAP axis in mesenchymal stem cells (MSCs) by both *in vitro* experiments and *in silico* computational model. The computational model predicted a mechanical PAR involving the bimodal distribution of focus adhesions, which enables cells to accurately perceive extracellular mechanical cues. Thus, our analysis of TGF-β1 mediated mechanosensing mechanism on MSCs may help to better understand the molecular process underlying bone regeneration.

INTRODUCTION

Recurring patterns in transcriptional regulation networks can be regarded as network motifs,[1] which play key roles in regulating cellular behaviors, e.g., proliferation, differentiation, and population.[2] The positive autoregulation (PAR) is a simple but important network motif, by which a protein can promote its own rate of production.[3] The characteristic feature of PAR is the maintenance of a bimodal distribution of the concentration of a certain protein (e.g., the typical chemical factor MAPK).[4] Usually, the bimodal distribution is thought to play important roles in phenotypic heterogeneity, which could mediate cellular adaptation to the changes in their microenvironments.[5] Besides biochemical factors (e.g., GTPases[6]), PAR has recently been acknowledged to sense and respond to typical mechanosensing proteins, indicating that PAR may also play key roles in mechanotransduction. For example, the integrin-YAP loop can be regarded as a typical mechanical PAR that is related to actin cytoskeleton and cell tension in cell mechanics.[7] Although the molecular feedback of the integrin-FAK-YAP axis has been extensively studied,[8,9] the role of such mechanical PAR in physiological development (e.g., differentiation) and pathological process (e.g., inflammation) remains elusive.

Bone defects are one of the global health problems caused by pathological bone resorption.[10–14] Both the biochemical and biophysical cues are involved in the process of bone resorption.[15] Accumulating evidence has suggested that elevated levels of integrin and transforming growth factor β (TGF-β) tend to appear along with the development of bone regeneration. Due to their ability of osteogenic lineage commitment, mesenchymal stem cells (MSCs) implantation has shown great promise to enhance bone regeneration in several clinical conditions.[16,17] As a biochemical cue, TGF-β controls MSCs differentiation by regulating downstream signaling pathways (e.g., MAPK and Smads) during bone formation and bone homeostasis.[14] Besides, integrin could also be upregulated in osteoblasts by TGF-β1 treatment.[18] Thus, we hypothesize that TGF-β1 can also influence the integrin mediated mechanical PAR for MSC mechanotransduction and osteogenesis. Unfortunately, the mechanisms of such a process are still unclear, hindering the MSC-based therapies for bone regeneration.

In this study, we found the decrease of both TGF-β1 and integrin levels as accompanied with decreasing tissue stiffness in rat model of periodontitis (an inflammatory disease with bone defect). Then, we investigated the roles of TGF-β1 and stiffness on osteogenesis of MSCs and examined integrin associated mechanosensitive signaling pathway during osteogenic differentiation of MSCs, using RGD and TGF-β1 aptamers modified PEG hydrogels with different stiffness as cell culture models. We found that TGF-β1 strengthens integrin

[1]Key Laboratory of Shaanxi Province for Craniofacial Precision Medicine Research, College of Stomatology, Xi'an Jiaotong University, Xi'an 710004 P.R. China
[2]Key Laboratory of Biomedical Information Engineering of Ministry of Education, School of Life Science and Technology, Xi'an Jiaotong University, Xi'an 710049 P.R. China
[3]Bioinspired Engineering and Biomechanics Center (BEBC), Xi'an Jiaotong University, Xi'an 710049 P.R. China
[4]State Key Laboratory of Military Stomatology & National Clinical Research Center for Oral Diseases & Shaanxi International Joint Research Center for Oral Diseases, Department of General Dentistry and Emergency, School of Stomatology, Fourth Military Medical University, Xi'an 710032 P.R. China
[5]Lead contact
*Correspondence: peidandan@xjtu.edu.cn (D.P.), minlin@xjtu.edu.cn (M.L.), chenbo8874@xjtu.edu.cn (B.C.)
https://doi.org/10.1016/j.isci.2024.110262

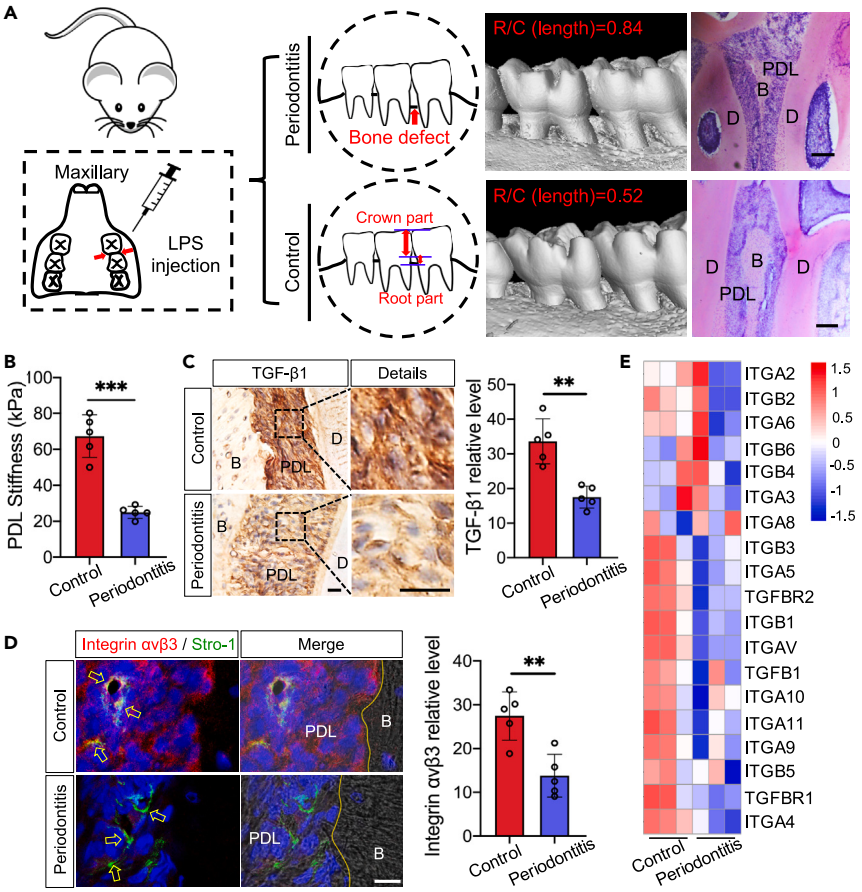

Figure 1. Decreased expression of TGF-β1 and integrin $\alpha_v\beta_3$ in the periodontal ligament (PDL) upon periodontitis

(A) Schematic of periodontitis induction between the first and second molar of rat maxillary. Both the MicroCT and HE staining indicated obvious absorption of alveolar bone caused by periodontitis (decreased R/C value and bone mass). Scale bar, 200 μm.

(B) The stiffness of healthy PDL and periodontitis PDL in rats.

(C) Immunostaining for TGF-β1 in healthy and periodontitis PDL of rats (left) and the corresponding quantification of TGF-β1 expression (right). Scale bar, 20 μm.

(D) Immunostaining for integrin $\alpha_v\beta_3$ and stro-1 expression in healthy and periodontitis PDL of rats (left) and corresponding quantification of integrin $\alpha_v\beta_3$ expression (right). Red, integrin $\alpha_v\beta_3$; green, stro-1, one of the markers for mesenchymal stem cells; blue, nucleus. Scale bar, 30 μm. (E) Meta-analysis of published gene expression omnibus (GEO) data analysis showing TGF-β1, TGF-β1 receptor, and integrin expression in healthy PDL and periodontitis PDL. R, root; C, crown; B, bone; D, dentin. ***$p < 0.001$, **$p < 0.01$.

mediated mechanical PAR, which induces the formation of bimodal distribution of adhesion length. Since nascent (small size) focal adhesions (FAs) mainly sense the mechanical properties of the local extracellular matrix by short turn-over time while mature (large size) FAs transmit mechanical signals by linking the extracellular matrix (ECM) and the intracellular F-actin,[19] the bimodal distribution of adhesion length may contribute to maintain the MSCs functions. Analysis of the crosstalk between integrin and TGF-β1 could help to better understand the molecular processes during MSC osteogenic differentiation, which contributes to MSC-based bone regeneration therapies. This TGF-β1 mediated mechanical PAR would be a promising target for explaining how cells respond to their microenvironment.

RESULTS

Development of paradentium *in vivo* decreases TGF-β1 and integrin levels

First, we investigated the levels of TGF-β1 and integrin $\alpha_v\beta_3$ in a rat model of periodontitis. The bone mass of the periodontitis group is lower than that of the control group, indicating obvious absorption of alveolar bone after periodontitis (Figures 1A and S1). The stiffness of periodontal ligament (PDL) in periodontitis rat decreases significantly compared with healthy PDL (Figure 1B). Compared with the control group, the levels of TGF-β1 and integrin $\alpha_v\beta_3$ in periodontitis PDL significantly decrease as reflected by both immunohistology and immunofluorescent staining (Figures 1C and 1D). These results were further confirmed in Gene Expression Omnibus (GEO) (accession number GSE27993) where low levels of both TGF-β1 and integrin $\alpha_v\beta_3$ could also be identified in periodontitis PDL, with a correlated expression during the

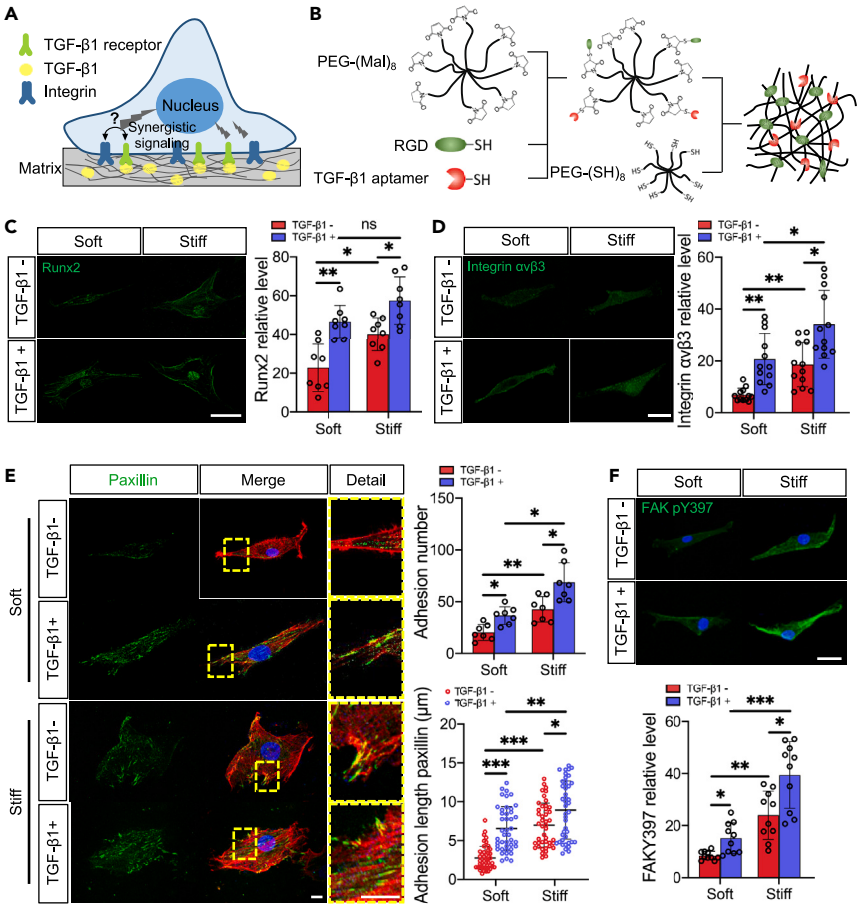

Figure 2. Integrin mediated adhesion formation and MSCs osteogenic differentiation correlated with substrate stiffness and TGF-β1

(A) Schematic of the design of cell experiment *in vitro* for MSCs osteogenesis regulated by TGF-β1 and integrin mediated signaling.

(B) Schematic of PEG hydrogel cross-linking process.

(C) Immunostaining of Runx2 expression in MSCs *w/wo* TGF-β1 on hydrogels with different stiffness and the quantification of Runx2 expression (right). Scale bar, 30 μm.

(D) Immunostaining of integrin $\alpha_v\beta_3$ expression in MSCs *w/wo* TGF-β1 on hydrogels with different stiffness and the quantification of integrin $\alpha_v\beta_3$ (right). Scale bar, 30 μm.

(E) Immunostaining of focal adhesion (FA; paxillin) in MSCs *w/wo* TGF-β1 on different stiffness hydrogels and the quantification of FA number (upper right) and FA length (lower right). Green, paxillin; red, F-actin; blue, nucleus. Scale bar, 10 μm.

(F) Immunostaining of FAK Y397 phosphorylation expression in MSCs *w/wo* TGF-β1 on different stiffness hydrogels and the quantification of FAK Y397 phosphorylation level (lower). Scale bar, 30 μm ***$p < 0.001$, **$p < 0.01$, *$p < 0.05$.

development of periodontitis (Figures 1E and S2). Given that the expressions of TGF-β1 and integrin $\alpha_v\beta_3$ are correlated with RUNX2, an osteogenic differentiation marker, these results indicate that the levels of TGF-β1 and integrin $\alpha_v\beta_3$ decrease with the development of paradentium and may be related to osteogenic differentiation.

The *in vitro* cellular microenvironment recapitulates native periodontium

To further investigate the synergistic effects of TGF-β1 and integrin $\alpha_v\beta_3$ in mediating the fate commitment of MSCs during the development of paradentium, we developed TGF-β1 aptamer modified PEG hydrogel to mimic native situations (Figure 2A). In order to mimic the states *in vivo*, we modulated matrix stiffness and TGF-β1 levels to simulate the periodontal microenvironments under different conditions. The stiffness of the PEG hydrogel substrate is tuned to 20 kPa ("soft") or 50 kPa ("stiff"), and the addition of TGF-β1 does not affect the stiffness (Figure S3A). Fluorescence results indicated that RGD and TGF-β1 aptamer are successfully modified onto the hydrogel (Figures 2B, S3B, and S3C). According to the ELISA results, the binding between TGF-β1 and aptamer increases gradually over time and reaches the highest bounding rate (>60%) at 4 h (Figures S3DS3E).

To prove the validity of the material, we assessed MSCs viability on PEG hydrogel *w/wo* RGD. Cell viability is significantly higher on RGD modified hydrogel than that without RGD (Figure S4A), further confirming that RGD is successfully modified onto the PEG hydrogel.

Besides, we characterized cell spreading on hydrogels with different stiffnesses *w/wo* TGF-β1 treatment. MSCs on stiff hydrogel with TGF-β1 show the largest spreading area, indicating a matrix stiffness and TGF-β1 dependent cell spreading (Figure S4B). Thus, a mechano-chemical coupling cell microenvironment has been successfully developed which recapitulates cellular microenvironment in native periodontium.

Substrate stiffness dependent adhesion formation and osteogenic differentiation of MSCs

Osteogenic differentiation of MSCs is mainly connected with bone regeneration.[20] Next, we investigated the osteogenic differentiation of MSCs driven by the synergistic effects of ECM stiffness and TGF-β1. The level of Runx2 is enhanced with increasing stiffness and TGF-β1 content as reflected by the immunofluorescence staining (Figure 2C). These results indicate that TGF-β1 and matrix stiffness could promote osteogenic differentiation of MSCs.

Later, we checked the expression of $\alpha_v\beta_3$ integrin of MSCs on different stiffness PEG hydrogels *w/wo* TGF-β1 treatment. The expression of $\alpha_v\beta_3$ integrin significantly increases with the increasing level of TGF-β1 and matrix stiffness as reflected by immunofluorescence staining (Figure 2D). Similarly, focal adhesion length and number, as characterized by paxillin, are also enhanced by increasing TGF-β1 and matrix stiffness (Figure 2E). Besides, FAK Y397 phosphorylation also increases with the increasing TGF-β1 and matrix stiffness (Figure 2F). All these observations indicate that both TGF-β1 and matrix stiffness could enhance the integrin-mediated adhesion formation to promote osteogenic differentiation of the MSCs.

TGF-β1 promotes integrin-YAP mediated mechanosensing

Accumulating evidence has suggested that YAP is an important regulator of cell differentiation,[21] where the nuclear/cytoplasmic shuttling of YAP is regulated by mechanical cues of ECM involving the formation of perinuclear apical actin cables on top of the nucleus.[22–24] Therefore, we asked whether TGF-β1 induces YAP nucleus translocation by triggering the formation of actin cap by flattening the nucleus. First, we found that YAP mainly remains in the cytoplasm for cells cultured on soft hydrogel without TGF-β1. When cells are cultured with the increased content of TGF-β1 or on stiff substrate, YAP begins to translocate into the nucleus (Figures 3A and 3B). Meanwhile, the fraction of MSCs with actin cap increases when subject to TGF-β1 or stiff substrate (Figures 3A and 3B). Besides, 3D-reconstructed confocal z-slices of the lamin A/C-immunostained nuclei showed that the nuclei are flattened gradually with TGF-β1 treatment or on stiff substrate (Figures 3A and 3B). Together, these results reveal that both TGF-β1 and substrate stiffness could promote the integrin-mediated reinforcement of actin cytoskeleton and nucleus flattening, which further induces YAP nucleus translocation.

To further investigate the synergistic effects of TGF-β1 and integrin mediated mechanotransduction on regulating YAP nuclear/cytoplasmic shuttling, we blocked FAKY397 (a key regulator downstream of integrin[25]) with FAK Y397 inhibitors (FP573228). We found that the phosphorylation level of FAK Y397 is effectively reduced with the treatment of inhibitor (Figure S5). Blocking FAK Y397 significantly decreases the YAP nuclear-to-cytoplasmic (nuc/cyto) ratio even for cells treated with TGF-β1, whereas the YAP nuc/cyto ratio does not present a significant decrease when culturing cells on soft substrate without TGF-β1 treatment (Figure 3C). Overall, TGF-β1 plays a positive role in integrin-mediated mechanosensing.

TGF-β1 induces the formation of integrin mediated mechanical PAR

Recently, studies have shown that integrin-YAP can also form a mechanical PAR.[7] Thus, to explore whether such feedback also works in TGF-β1 driven integrin-YAP signaling axis (Figure 4A), we knocked down YAP in MSCs by using small interfering RNA (siRNA) (Figure S6). siRNA treated MSCs cultured either on soft or stiff hydrogels display impaired FA maturation (Figures 4B and 4C), confirming the role of mechanical PAR in TGF-β1 driven integrin-YAP signaling axis.[7] These results were also confirmed in verteporfin experiment (Figure S7).

To investigate the effects of TGF-β1 on integrin mediated mechanical PAR, we next cultured siYAP MSCs on soft/stiff substrate with TGF-β1 treatment. We observed that FA maturation is significantly decreased in siRNA treated MSCs even after TGF-β1 treatment on stiff substrate (Figures 4B, 4C, and S8). Besides, FA related proteins are also reduced compared with control groups (Figures 4D–4F). Integrin downstream key regulator, such as FAK Y397, also changes significantly after the silencing of YAP (Figure S9). These results indicate that TGF-β1 induces the formation of integrin mediated mechanical autoregulation through the regulation of YAP. Besides, the stiff substrate also enhanced TGF-β1expression (Figure S10), which in turn increased mechanical PAR to a certain extent.

Mechanical PAR induces bimodal distribution of FA length

To further investigate the role of integrin-YAP-mediated mechanical PAR in cellular behavior, we developed a mathematical model based on our experimental data. Here, we hypothesized that TGF-β1 could induce mechanical PAR formation involving the integrin-FAK-YAP axis in normal MSCs, but there is no mechanical PAR formation in disease states (periodontitis) with low stiffness and low levels of TGF-β1 (Figure 5A). Based on the aforementioned hypothesis, we developed a mathematical model to describe this process, which includes the expression of the ITGB1 gene, the degradation of the integrin protein, the nucleoplasmic shuttling process of YAP, the YAP-mediated state change of the gene, and the clustering process of the integrin (Figure 5B, see STAR Methods section for a detailed description).

Then, to confirm the existence of unimodal and bimodal distributions in the experimental data, we used the k-density function in MATLAB to fit the sample data distribution. The results showed that there was only one peak of FA distribution on the soft matrix, which was mostly composed of small adhesions (Figure 5C). The bimodal distribution of FA length represents a diversity distribution in cells on the stiff

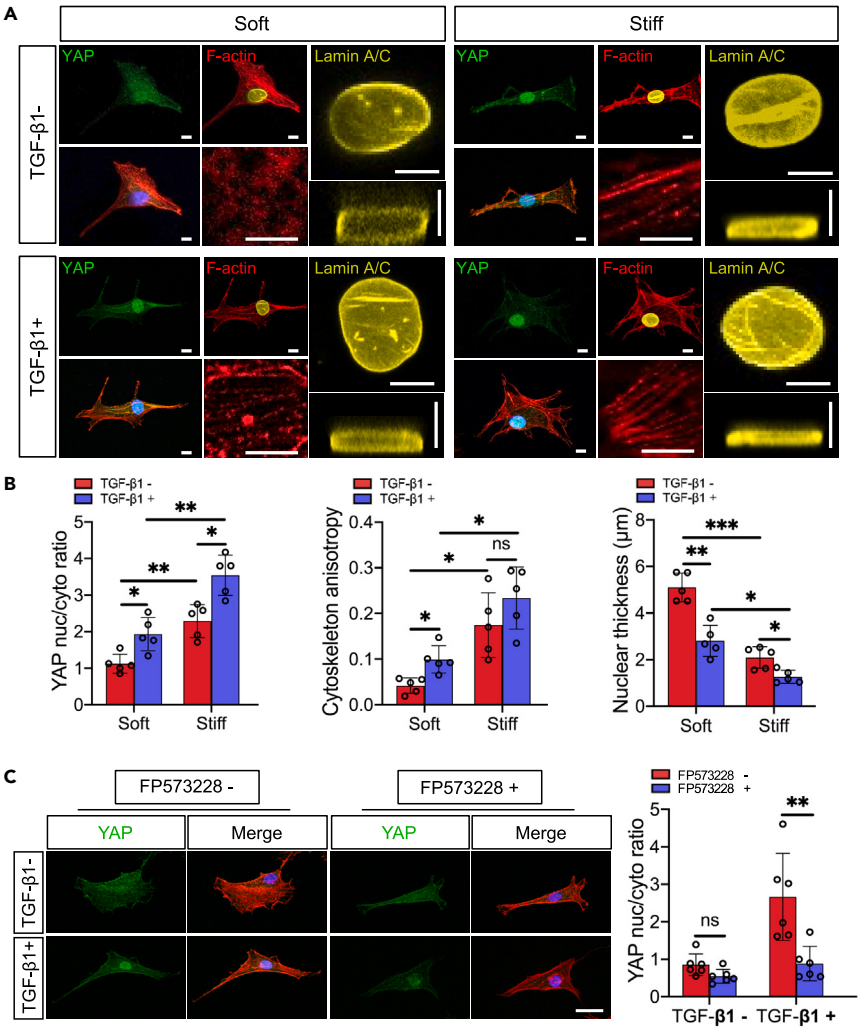

Figure 3. TGF-β1 promoted the integrin-YAP mediated mechanosensing pathway

(A) Representative immunofluorescent images of YAP, F-actin, and nuclear lamin A/C-in MSCs w/wo TGF-β1 treatment or on different stiffness hydrogels. Green, YAP; red, F-actin; yellow, lamin A/C; blue, nucleus. Scale bar, 10 μm.

(B) Quantification of YAP nuclear/cytoplasm ratio, cytoskeleton anisotropy, and nuclear thickness.

(C) Immunostaining of YAP nuclear localization in MSCs after the inhibition of FAK Y397 *w/wo* TGF-β1 on soft hydrogel and quantification of YAP nuclear/cytoplasm ratio (right). Green, YAP; red, F-actin; blue, nucleus. Scale bar, 30 μm ***$p < 0.001$, **$p < 0.01$, *$p < 0.05$.

substrates, where only parts of the FAs become larger, while others remain small even after the addition of TGF-β1. Consistent with the experimental results, the mathematical model simulation results again showed that the FA length distribution shifts from unimodal to bimodal with the change of parameter corresponding to increased stiffness or TGF-β1 treatment (Figure 5D). For this result, we chose the model parameters $\alpha = 0.1$, $\beta = 1$ to match the experimental phenomenon, indicating that matrix stiffness had less weight in our experiment. However, due to the positive mechanical feedback mediated by matrix stiffness, when TGF-β induced integrin protein increased, the mechanical feedback played a further role in enhancing integrin expression and matured most of the adhesion.

Later, we performed a sensitivity analysis of the model parameters (Figures S11S19). In general, the distribution of FA can be categorized into 2 types as the parameters are changed: unimodal distribution and bimodal distribution. With successive parameter changes, the unimodal distribution of nascent (small) FAs gradually transitions to a bimodal distribution (coexistence of small and large FAs) to the unimodal distribution of large FAs, and vice versa (Figure 5E). Specifically, increasing the basal expression rate (r_1) of genes, cytoplasmic YAP protein number (C_yap) and YAP-mediated gene activate rate (r_2) induced cell adhesion maturation; increasing gene deactivate rate (r_3), the degradation rate of integrins (r_5), and the YAP nuclear out-rate (r_7) inhibited cell adhesion maturation. In addition, we found that the process of integrin expression, clustering, and mechanical positive feedback can promote the maturation of cell adhesion (such as by increasing r_1, r_2, k, K_H, and C_{yap}), which is manifested by the formation of bimodal distribution or single peak distribution of mature adhesion (Figure 5E).

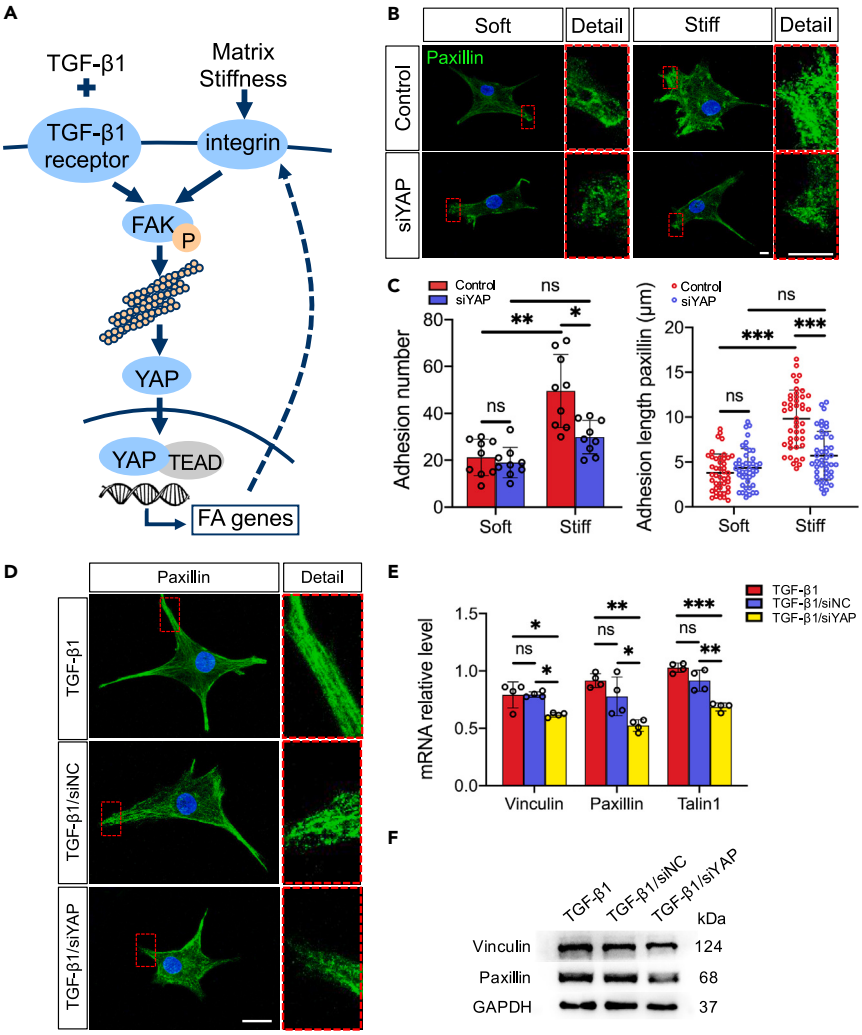

Figure 4. TGF-β1 mediated integrin-YAP mechanical positive autoregulation (PAR)

(A) Schematic of the proposed pathway of TGF-β1 mediated integrin-YAP mechanical PAR.

(B) Immunostaining of FA (paxillin) expression in YAP silenced-MSCs on different stiffness hydrogels. Green, paxillin; blue, nucleus. Scale bar, 10 μm.

(C) Quantification of the FA number (left) and FA length (right).

(D) Immunofluorescent staining of FA (paxillin) expression in YAP silenced-MSCs with TGF-β1 treatment on the stiff hydrogel. Green, paxillin; blue, nucleus. siNC, control siRNA group. Scale bar, 10 μm.

(E) Real-time PCR analysis of FA related genes expression in YAP silenced-MSCs with TGF-β1 treatment on stiff hydrogel, including vinculin, paxillin and talin1.

(F) Western blot analysis of FA related protein expression in YAP silenced-MSCs with TGF-β1 treatment on stiff hydrogel, including vinculin, paxillin, and talin1.

***$p < 0.001$, **$p < 0.01$, *$p < 0.05$.

For different expression rates of activated genes (k from 1 to 100), a higher expression rate of ITGB1 in the active gene significantly promoted the transition from nascent adhesions to mature and larger adhesions. A bimodal distribution occurred when the approximate expression rate of the activated gene was about 10 times the expression rate of the basal state of the gene (Figure S14).

Since substrate stiffness and TGF-β can both promote integrin expression, in our sensitivity analysis, we assume that stiffness and TGF-β have the different strength for integrin-mediated YAP nuclear entry, i.e., the ratio of coefficients of parameters S and T are $\alpha/\beta = 0.1–10$ in the mathematical model. We found that increasing the stiffness-dependent weights made the cells more likely to form mature adhesions. Interestingly, however, on soft substrates with TGF-β, the cells showed only a bimodal distribution over the range of parameters we chose (Figure S17).

Mathematical simulation showed that TGF-β1 can enhance integrin-mediated mechanical PAR, which induces the formation of bimodal distribution of adhesion length and unimodal distribution for large FA. MSCs use small size FAs to sense local ECM stiffness and large size FAs to transmit stable mechanical signals. Both types of FAs lead to continuous and efficient osteogenic differentiation of MSCs (Figure 5F). Thus, analyzing the crosstalk between integrin and TGF-β1 leads to a better understanding of the molecular processes underlying MSC osteogenic differentiation.

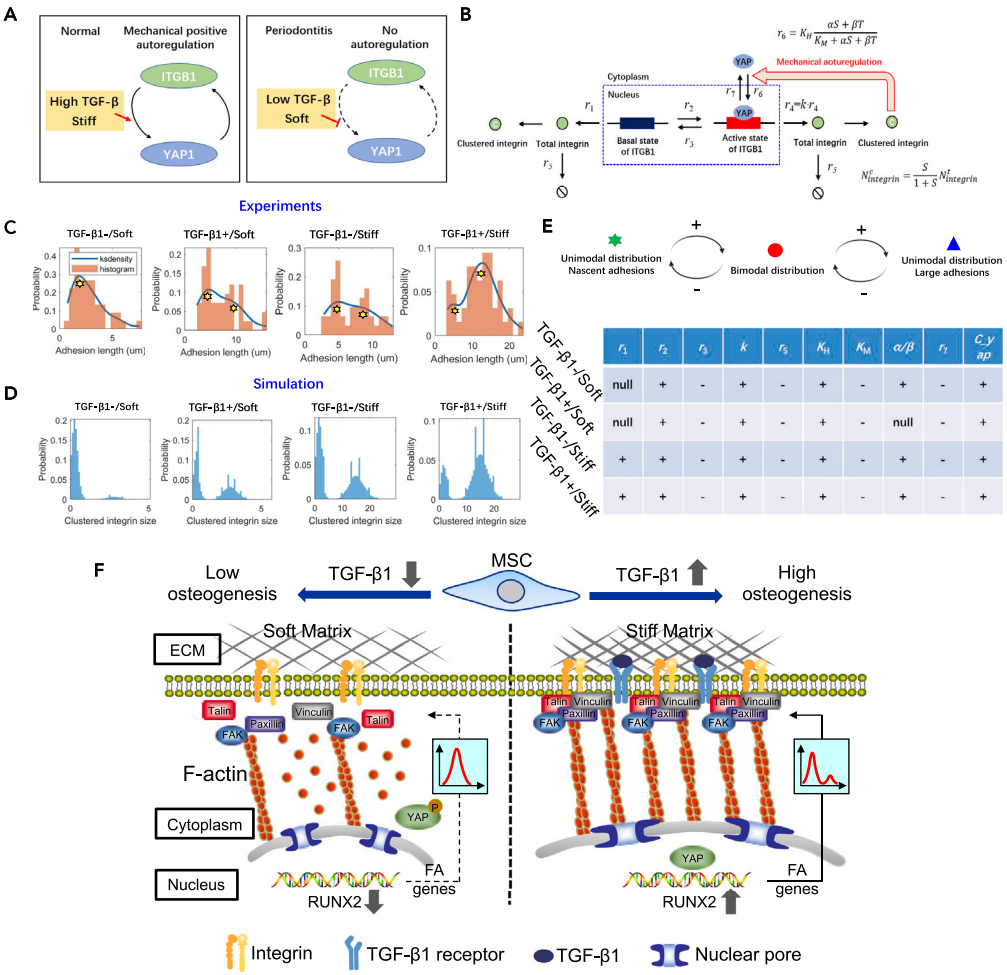

Figure 5. TGF-β1 and matrix stiffness mediated mechanical positive autoregulation (PAR) could induce the bimodal distribution of FA

(A) Model assumption of PAR for mathematical model.

(B) Schematic of the mathematical model.

(C and D) The distribution evolution of FA length (clustered integrins) in our experiments and simulation.

(E) The sensitivity analysis of the mathematical model. + represents a forward process in which the distribution changes as the parameter value increases; - represents a reverse process in which the distribution changes as the parameter value increases.

(F) A schematic illustration of TGF-β1 and matrix stiffness induced the formation of integrin mediated mechanical PAR by YAP. TGF-β1 and stiff matrix activate focal adhesion proteins-talin, vinculin, and paxillin, they bind to and activate integrin, resulting in downstream mechanical signaling, such as FAK. This mechanical signaling creates tension on the actin fiber cytoskeleton which causes stretching of the nuclear pore and ensures nuclear localization of YAP. In the nucleus, YAP promotes the transcription of genes encoding for FA proteins. The successive feedback induces integrin mediated mechanical PAR. On the contrary MSCs on the soft substrate without TGF-β1 treatment experience less tension, forming an unstable focal adhesion complex. Tension-dependent stretching of actin fiber cytoskeleton is disrupted, causing cytoplasmic retention of YAP and less mechanical PAR.

DISCUSSION

Both biochemical and biophysical factors can form PAR, which plays key roles in the regulation of cellular behaviors (e.g., differentiation). During the process of periodontitis, changes in biochemical factors (e.g., GFs, inflammatory cytokines) and biophysical factors (e.g., stiffness, viscoelasticity) in cell microenvironment usually lead to the destruction of alveolar bone. Both TGF-β1 and integrins in periodontal ligament were found in this study to decrease in rats of periodontitis. However, the mechanism of mechanical PAR in this bone resorption process remains elusive. Therefore, we treated MSCs with different concentrations of TGF-β1 and matrix stiffness to mimic the *in vivo* situation and investigated the role of TGF-β1 in mediating mechanical PAR *in vitro*.

TGF-β is a key biochemical stimulus that promotes multiple cell functions, such as cellular proliferation, migration, and differentiation.[26] In many studies, TGF-β is usually mixed into cell culture solution, which cannot fully reflect the native microenvironment. Besides, due to the diffusion of solute TGF-β, the concentration of TGF-β is usually high which makes it inefficient and unsafe. Compared to the soluble form of TGF-β, the solid-phase presentation of TGF-β results in higher efficiency, which improves biological functions and reduces concentration

and does.[27] In addition, the solid-phase presentation has a better control of TGF-β spatial distribution to target their receptors.[28] Therefore, we chose solid-phase TGF-β1 presentation in this study by coating PEG hydrogels with TGF-β1 aptamer, which can then bind to TGF-β1 protein. In this way, the engineered biochemical microenvironment of MSCs is much closer to the physiological condition.

Recent studies have found that extracellular biochemical factor-dependent biochemical signaling pathways can interact with biophysical signal transduction pathways to further affect the differentiation behavior of MSCs. For example, BMP-2 signaling needs to cooperate with the biophysical signaling of the ECM at the transcriptional level to regulate the osteogenic differentiation of MSCs. Activation of osteogenic genes requires the BMP-2 pathway-related Smad1/5/8 heteromeric complex and mechanosensitive YAP/TAZ synergies to promote the nuclear translocation of YAP/TAZ, which in turn drives the osteogenic differentiation of cells.[29] TGF-β/BMP receptors could either sense biophysical properties of ECM directly, or they participate in transforming these parameters into cell fate changes.[30] Furthermore, interactions between BMP receptors and integrins have multiple effects, highlighting the dependence on the crosstalk between integrin and BMP.[31–33] As a member of the TGF-β superfamily, our study also found that there is crosstalk between TGF-β1 and integrins signaling.

Our results demonstrated that (i) TGF-β1 promotes MSCs osteogenic differentiation and maintains bone mass by activating both the biochemical and biophysical signalings, and (ii) TGF-β1 helps promote the feedback of integrin mediated mechanical PAR, which could induce the bimodal distribution of focal adhesion (FA). In our study, the expression of integrin $\alpha_v\beta_3$ was found to be up-regulated by TGF-β1 signaling. As a major family member of transmembrane receptors responsible for cell adhesion, integrin $\alpha_v\beta_3$ can assemble cell-matrix adhesions via the formation of FAs providing a mechanical link between the ECM and intracellular actin fibers.[34] Our results demonstrate that TGF-β1 signaling induces activation of mechanosensation signaling including the activation of FAK Y397, enhancement of actin fiber, nucleus flattening and YAP nucleus translocation, forming the mechanical PAR and leading to the improvement of osteogenic differentiation.

Furthermore, the enhanced TGF-β1expression by stiff substrate also in turn increased mechanical PAR to a certain extent.

YAP plays key roles in regulating adhesion-mediated cell mechanosensing.[7] MSCs showed impaired FA maturation upon YAP silence. Thus, these feedback loops mediated by YAP are processes that connect input signals (e.g., matrix stiffness) back to their outputs (e.g., FA and integrin). Thus, the structure of mechanical PAR is such that integrin influences its own level and regulates itself via a feedback loop mediated by YAP signaling. Besides, TGF-β1 could enhance this mechanical PAR by promoting YAP nucleus localization.

PAR has been found in multiple systems, and the bi-stability is one of the characteristics of the PAR pattern, which means that there are two stable steady states in the regulation.[2,35,36] In the bi-stable system, one steady state generally corresponds to a "close state", and the other one is an "open state". For example, in the cell cycle control systems of eukaryotes, low and high activities of the kinase Cdc2 contribute to the interphase and mitosis respectively.[37] Besides, the levels of key molecules in the bi-stable system are likely characterized by a bimodal distribution.[38] In our study, the FA length displayed bimodal distribution when cells were exposed to varied TGF-β1 concentrations and matrix stiffnesses. Parts of FAs kept high gathering while others maintained the "bridge" function. Bimodal distribution of gene products can lead to cell phenotypic diversity which contributes to a better population adaption in a complex and changing microenvironment.[5] Usually, a balanced homeostasis exists in healthy periodontal microenvironments. Once this balance is disrupted, inflammation can be triggered leading to periodontitis. This bimodal distribution phenomenon also aids cells in coping with the complex periodontal microenvironment and may play a key role in maintaining periodontal homeostasis, offering new strategies and theoretical support for the prevention and treatment of periodontitis. The mechanism of the bimodal distribution in this study needs to be further explored in further studies.

Limitations of the study

Our mathematical model still suffers from the following limitations: First, in our experiments, both stiffness and TGF-β can promote integrin-mediated YAP nuclear entry, but we are currently unable to distinguish the strength between these two factors in the aforementioned process. Therefore, for simplicity, we assume that stiffness and TGF-β have different strengths (the coefficients of parameters S and T), which should be validated by experiments. Second, some studies have shown that the time delay between transcription and translation has effects on gene expression, such as stochastic oscillation or a bistable state. However, since we have not experimentally characterized these two processes in the existing study, we do not consider the effects of translational delay in our mathematical model for now. The delayed effects of the latter transcriptional processes on cellular mechanosensing need to be further investigated in related studies. Besides, we measured the TGF-β1 expression on different stiffnesses only in our experiments, and our model analysis has not yet considered how matrix stiffness regulates the expression of TGF-β1. TGF-β1 is primarily thought to be a changeable external condition in the extracellular matrix, which is used as an input parameter for the model analysis. Further research of the model analysis could incorporate the differences autocrine TGF-β1 in MSCs caused by extracellular matrix stiffness.

STAR★METHODS

Detailed methods are provided in the online version of this paper and include the following:

- KEY RESOURCES TABLE
- RESOURCE AVAILABILITY
  - Lead contact
  - Materials availability
  - Data and code availability

SUPPLEMENTAL INFORMATION

Supplemental information can be found online at https://doi.org/10.1016/j.isci.2024.110262.

ACKNOWLEDGMENTS

This work was supported in part by the National Natural Science Foundation of China (12022206, 11972280, and 81970981), Natural Science Basic Research Program of Shaanxi (2024JC-YBQN-0959), and Openning Project of Key Laboratory of Shaanxi Province for Craniofacial Precision Medicine Research, College of Stomatology, Xi'an Jiaotong University (2020LHM-KFKT001).

AUTHOR CONTRIBUTIONS

Conceptualization, B.C., M.L., and P.D.; methodology, W.W., B.C., and F.X.; investigation, W.W. and H.Z.; validation, L.N.; writing – original draft, W.W. and M.Z.; writing – review and editing, W.W., B.C., M.L., and P.D.; resources, F.X., A.L., and M.L.; supervision, B.C., M.L., and P.D. All authors have read and approved the final manuscript.

DECLARATION OF INTERESTS

The authors declare no competing interest.

Received: November 16, 2023
Revised: April 18, 2024
Accepted: June 10, 2024
Published: June 12, 2024

REFERENCES

1. Alon, U. (2007). Network motifs: theory and experimental approaches. Nat. Rev. Genet. *8*, 450–461. https://doi.org/10.1038/nrg2102.
2. Mitrophanov, A.Y., and Groisman, E.A. (2008). Positive feedback in cellular control systems. Bioessays *30*, 542–555. https://doi.org/10.1002/bies.20769.
3. Schreier, H.I., Soen, Y., and Brenner, N. (2017). Exploratory adaptation in large random networks. Nat. Commun. *8*, 14826. https://doi.org/10.1038/ncomms14826.
4. Paliwal, S., Iglesias, P.A., Campbell, K., Hilioti, Z., Groisman, A., and Levchenko, A. (2007). MAPK-mediated bimodal gene expression and adaptive gradient sensing in yeast. Nature *446*, 46–51. https://doi.org/10.1038/nature05561.
5. Ochab-Marcinek, A., and Tabaka, M. (2010). Bimodal gene expression in noncooperative regulatory systems. Proc. Natl. Acad. Sci. USA *107*, 22096–22101. https://doi.org/10.1073/pnas.1008965107.
6. Goryachev, A.B., and Leda, M. (2019). Autoactivation of small GTPases by the GEF-effector positive feedback modules. F1000Res. *8*, 1676. https://doi.org/10.12688/f1000research.20003.1.
7. Nardone, G., Oliver-De La Cruz, J., Vrbsky, J., Martini, C., Pribyl, J., Skládal, P., Pešl, M., Caluori, G., Pagliari, S., Martino, F., et al. (2017). YAP regulates cell mechanics by controlling focal adhesion assembly. Nat. Commun. *8*, 15321. https://doi.org/10.1038/ncomms15321.
8. Panciera, T., Azzolin, L., Cordenonsi, M., and Piccolo, S. (2017). Mechanobiology of YAP and TAZ in physiology and disease. Nat. Rev. Mol. Cell Biol. *18*, 758–770. https://doi.org/10.1038/nrm.2017.87.
9. Zhang, C., Zhu, H., Ren, X., Gao, B., Cheng, B., Liu, S., Sha, B., Li, Z., Zhang, Z., Lv, Y., et al. (2021). Mechanics-driven nuclear localization of YAP can be reversed by N-cadherin ligation in mesenchymal stem cells. Nat. Commun. *12*, 6229. https://doi.org/10.1038/s41467-021-26454-x.
10. Arumugam, B., Vairamani, M., Partridge, N.C., and Selvamurugan, N. (2018). Characterization of Runx2 phosphorylation sites required for TGF-β1-mediated stimulation of matrix metalloproteinase-13 expression in osteoblastic cells. J. Cell. Physiol. *233*, 1082–1094. https://doi.org/10.1002/jcp.25964.
11. Yu, L., Hébert, M.C., and Zhang, Y.E. (2002). TGF-beta receptor-activated p38 MAP kinase

mediates Smad-independent TGF-beta responses. EMBO J. *21*, 3749–3759. https://doi.org/10.1093/emboj/cdf366.
12. Isomursu, A., Lerche, M., Taskinen, M.E., Ivaska, J., and Peuhu, E. (2019). Integrin signaling and mechanotransduction in regulation of somatic stem cells. Exp. Cell Res. *378*, 217–225. https://doi.org/10.1016/j.yexcr.2019.01.027.
13. Marie, P.J. (2013). Targeting integrins to promote bone formation and repair. Nat. Rev. Endocrinol. *9*, 288–295. https://doi.org/10.1038/nrendo.2013.4.
14. Wu, M., Chen, G., and Li, Y.P. (2016). TGF-beta and BMP signaling in osteoblast, skeletal development, and bone formation, homeostasis and disease. Bone Res. *4*, 16009. https://doi.org/10.1038/boneres.2016.9.
15. Wan, W., Cheng, B., Zhang, C., Ma, Y., Li, A., Xu, F., and Lin, M. (2019). Synergistic effect of matrix stiffness and inflammatory factors on osteogenic differentiation of MSC. Biophys. J. *117*, 129–142. https://doi.org/10.1016/j.bpj.2019.05.019.
16. Dangaria, S.J., Ito, Y., Luan, X., and Diekwisch, T.G.H. (2011). Successful periodontal ligament regeneration by periodontal progenitor preseeding on natural tooth root surfaces. Stem Cells Dev. *20*, 1659–1668. https://doi.org/10.1089/scd.2010.0431.
17. Shinagawa-Ohama, R., Mochizuki, M., Tamaki, Y., Suda, N., and Nakahara, T. (2017). Heterogeneous human periodontal ligament-committed progenitor and stem cell populations exhibit a unique cementogenic property under in vitro and in vivo conditions. Stem Cells Dev. *26*, 632–645. https://doi.org/10.1089/scd.2016.0330.
18. Nesti, L.J., Caterson, E.J., Wang, M., Chang, R., Chapovsky, F., Hoek, J.B., and Tuan, R.S. (2002). TGF-beta1 calcium signaling increases alpha5 integrin expression in osteoblasts. J. Orthop. Res. *20*, 1042–1049. https://doi.org/10.1016/S0736-0266(02)00020-7.
19. Henning Stumpf, B., Ambrović-Ristov, A., Radenovic, A., and Smith, A.S. (2020). Recent advances and prospects in the research of nascent adhesions. Front. Physiol. *11*, 574371. https://doi.org/10.3389/fphys.2020.574371.
20. Lu, L., Liu, Y., Zhang, X., and Lin, J. (2020). The therapeutic role of bone marrow stem cell local injection in rat experimental periodontitis. J. Oral Rehabil. *47*, 73–82. https://doi.org/10.1111/joor.12843.
21. Virdi, J.K., and Pethe, P. (2021). Biomaterials regulate mechanosensors YAP/TAZ in stem cell growth and differentiation. Tissue Eng. Regen. Med. *18*, 199–215. https://doi.org/10.1007/s13770-020-00301-4.
22. Dupont, S. (2016). Role of YAP/TAZ in cell-matrix adhesion-mediated signalling and mechanotransduction. Exp. Cell Res. *343*, 42–53. https://doi.org/10.1016/j.yexcr.2015.10.034.
23. Kim, J.K., Louhghalam, A., Lee, G., Schafer, B.W., Wirtz, D., and Kim, D.H. (2017). Nuclear lamin A/C harnesses the perinuclear apical actin cables to protect nuclear morphology. Nat. Commun. *8*, 2123. https://doi.org/10.1038/s41467-017-02217-5.
24. Elosegui-Artola, A., Andreu, I., Beedle, A.E.M., Lezamiz, A., Uroz, M., Kosmalska, A.J., Oria, R., Kechagia, J.Z., Rico-Lastres, P., Le Roux, A.L., et al. (2017). Force triggers YAP nuclear entry by regulating transport across nuclear pores. Cell *171*, 1397–1410.e14. https://doi.org/10.1016/j.cell.2017.10.008.
25. Cheng, B., Wan, W., Huang, G., Li, Y., Genin, G.M., Mofrad, M.R.K., Lu, T.J., Xu, F., and Lin, M. (2020). Nanoscale integrin cluster dynamics controls cellular mechanosensing via FAKY397 phosphorylation. Sci. Adv. *6*, eaax1909. https://doi.org/10.1126/sciadv.aax1909.
26. Cipitria, A., and Salmeron-Sanchez, M. (2017). Mechanotransduction and growth factor signalling to engineer cellular microenvironments. Adv. Healthc. Mater. *6*, 1700052. https://doi.org/10.1002/adhm.201700052.
27. Diomede, F., Caputi, S., Merciaro, I., Frisone, S., D'Arcangelo, C., Piattelli, A., and Trubiani, O. (2014). Pro-inflammatory cytokine release and cell growth inhibition in primary human oral cells after exposure to endodontic sealer. Int. Endod. J. *47*, 864–872. https://doi.org/10.1111/iej.12230.
28. de Jong, T., Bakker, A.D., Everts, V., and Smit, T.H. (2017). The intricate anatomy of the periodontal ligament and its development: Lessons for periodontal regeneration. J. Periodontal. Res. *52*, 965–974. https://doi.org/10.1111/jre.12477.
29. Wei, Q., Holle, A., Li, J., Posa, F., Biagioni, F., Croci, O., Benk, A.S., Young, J., Noureddine, F., Deng, J., et al. (2020). BMP-2 signaling and mechanotransduction synergize to drive osteogenic differentiation via YAP/TAZ. Adv. Sci. *7*, 1902931. https://doi.org/10.1002/advs.201902931.
30. Ozdamar, B., Bose, R., Barrios-Rodiles, M., Wang, H.R., Zhang, Y., and Wrana, J.L. (2005). Regulation of the polarity protein Par6 by TGFbeta receptors controls epithelial cell plasticity. Science *307*, 1603–1609. https://doi.org/10.1126/science.1105718.
31. Kang, P.H., Schaffer, D.V., and Kumar, S. (2020). Angiomotin links ROCK and YAP signaling in mechanosensitive differentiation of neural stem cells. Mol. Biol. Cell *31*, 386–396. https://doi.org/10.1091/mbc.E19-11-0602.
32. Ashe, H.L. (2016). Modulation of BMP signalling by integrins. Biochem. Soc. Trans. *44*, 1465–1473. https://doi.org/10.1042/BST20160111.
33. Wang, Y.K., Yu, X., Cohen, D.M., Wozniak, M.A., Yang, M.T., Gao, L., Eyckmans, J., and Chen, C.S. (2012). Bone morphogenetic protein-2-induced signaling and osteogenesis is regulated by cell shape, RhoA/ROCK, and cytoskeletal tension. Stem Cells Dev. *21*, 1176–1186. https://doi.org/10.1089/scd.2011.0293.
34. Zuidema, A., Wang, W., Kreft, M., Te Molder, L., Hoekman, L., Bleijerveld, O.B., Nahidiazar, L., Janssen, H., and Sonnenberg, A. (2018). Mechanisms of integrin αVβ5 clustering in flat clathrin lattices. J. Cell Sci. *131*, jcs221317. https://doi.org/10.1242/jcs.221317.
35. Wykoff, D.D., Rizvi, A.H., Raser, J.M., Margolin, B., and O'Shea, E.K. (2007). Positive feedback regulates switching of phosphate transporters in S. cerevisiae. Mol. Cell *27*, 1005–1013. https://doi.org/10.1016/j.molcel.2007.07.022.
36. Igoshin, O.A., Price, C.W., and Savageau, M.A. (2006). Signalling network with a bistable hysteretic switch controls developmental activation of the sigma transcription factor in Bacillus subtilis. Mol. Microbiol. *61*, 165–184. https://doi.org/10.1111/j.1365-2958.2006.05212.x.
37. Sha, W., Moore, J., Chen, K., Lassaletta, A.D., Yi, C.S., Tyson, J.J., and Sible, J.C. (2003). Hysteresis drives cell-cycle transitions in Xenopus laevis egg extracts. Proc. Natl. Acad. Sci. USA *100*, 975–980. https://doi.org/10.1073/pnas.0235349100.
38. Becskei, A., Séraphin, B., and Serrano, L. (2001). Positive feedback in eukaryotic gene networks: cell differentiation by graded to binary response conversion. EMBO J. *20*, 2528–2535. https://doi.org/10.1093/emboj/20.10.2528.
39. Cheng, B., Li, M., Wan, W., Guo, H., Genin, G.M., Lin, M., and Xu, F. (2023). Predicting YAP/TAZ nuclear translocation in response to ECM mechanosensing. Biophys. J. *122*, 43–53. https://doi.org/10.1016/j.bpj.2022.11.2943.

STAR★METHODS

KEY RESOURCES TABLE

REAGENT or RESOURCE	SOURCE	IDENTIFIER
Antibodies		
anti-TGF-β1 antibody	Abcam	ab315254
anti-integrin alpha V + beta 3 antibody	GeneTex	GTX01084
anti-STRO-1 antibody	Invitrogen	14-6688-82
anti-Runx2 antibody	Abcam	ab76956
anti-paxillin antibody	Abcam	ab32084
anti-phospho-FAK antibody	Abcam	ab81298
anti-YAP antibody	Cell Signaling Technology	Cat# 14074
anti-lamin A/C antibody	Cell Signaling Technology	Cat# 4777
anti-vinculin antibody	Cell Signaling Technology	Cat# 13901
anti-FAK antibody	Cell Signaling Technology	Cat# 3285
anti-GAPDH antibody	Cell Signaling Technology	Cat# 2118
Chemicals, peptides, and recombinant proteins		
lipopolysaccharides(LPS)	Solarbio	L8880
MSCs specific growth medium	Cyagen	HUXMA-90011
OCT	SAKURA	4583
8-arm PEG maleimide	JenKem Technology	N/A
8-arm PEG thiol	JenKem Technology	N/A
rhodamine-labeled Arg-Gly-Asp	Sangon Biotech	N/A
FAM-labeled TGF-β1 aptamer	Sangon Biotech	N/A
recombinant human TGF beta 1 protein	Proteintech	Cat# HZ-1011
live/dead fluorescent dyes	Invitrogen	L3224
Alexa Fluor 594	Cell Signaling Technology	Cat# 8890
Alexa Fluor 488	Abcam	ab150077
DAPI	Cell Signaling Technology	Cat# 4083
Lipofectamine® 2000 reagent	Life Technologies	11668019
Opti-MEM medium	Life Technologies	31985070
verteporfin	Sigma	SML0534
Critical commercial assays		
human TGF-beta1 ELISA kit	Proteintech	Cat# KE00002
streptavidin-HRP kit	CWBIO	CW2069S
TaKaRa MiniBEST Universal RNA Extraction Kit	TaKaRa Bio	9767
PrimeScript RT Reagent Kit	TaKaRa Bio	RR047A
SYBR Premix Ex Taq II Kit	TaKaRa Bio	RR420A
Deposited data		
GEO database	National Center for Biotechnology Information	https://www.ncbi.nlm.nih.gov/geo/query/acc.cgi?acc=GSE27993
mathematical model codes	GitHub	https://github.com/cbcbcbcb123/Papers-Codes-Integrin-Mediated-Mechanical-Positive-Autoregulation.git

(*Continued on next page*)

Continued

REAGENT or RESOURCE	SOURCE	IDENTIFIER
Experimental models: Cell lines		
Mesenchymal Stem Cells	Cyagen	HUXMA-01001
Experimental models: Organisms/strains		
Sprague Dawley rats	Department of Laboratory Animal Science at Xi'an Jiaotong University	N/A
Oligonucleotides		
Primer for real-time PCR	Sangon Biotech	N/A
siRNA	GenePharma	N/A
Software and algorithms		
Image J	NIH	N/A
Graphpad Prism 8	GraphPad Software	N/A
Origin	Origin Software	N/A
Matlab	Matlab Software	N/A

RESOURCE AVAILABILITY

Lead contact

Further information and requests for resources and reagents should be directed to and will be fulfilled by the lead contact, Bo Cheng (chenbo8874@xjtu.edu.cn).

Materials availability

This study did not generate new unique reagents.

Data and code availability

- Paper analyzes existing, publicly available data. These accession numbers for the datasets are listed in the key resources table. All data reported in this paper will be shared by the lead contact upon request.
- All the custom computer code is available in this paper's supplemental information.
- Any additional information required to reanalyze the data reported in this paper is available from the lead contact upon request.

EXPERIMENTAL MODEL AND STUDY PARTICIPANT DETAILS

Rat model

Twenty 6-week-old healthy male Sprague-Dawley (SD) rats (200±50 g) were raised in the Department of Laboratory Animal Science at Xi'an Jiaotong University in stable environmental conditions (23°C, 40% relative humidity, a light-dark cycle of 12 h and free access to food and water). The experimental protocol followed the guidelines provided by the Care and Use of Laboratory Animals of Xi'an Jiaotong University. Each animal was intraperitoneally injected with 10% chloral hydrate to induce and maintain anesthesia during the experiment. All applicable institutional guidelines for the care and use of animals were followed. All animal procedures were approved by the Biomedical Ethics Committee of Health Science Center of Xi'an Jiaotong University (No. XJTUAE2023-1280).

10 μL Pg-LPS (1 mg/mL; Solarbio, Beijing, China) was injected into the palatal gingiva between the first and second molars on the left side of the maxilla using a microliter syringe (Gaoge, Shanghai, China). Meanwhile, 10 μL saline solution was injected into the same place on the right side as a control. This injection was performed at 48 h intervals. Periodontitis was inducted after 14 d with a total of 6 injections of Pg-LPS. Then, rats were euthanized and maxillae were harvested and hemisected (periodontitis side and the control side). Randomized parts of fresh maxillae were used for PDL stiffness analysis and parts were stored in 70% ethanol for micro-CT analysis. Other maxillae were fixed using 4% paraformaldehyde for the following histology analysis.

Cell culture

Human bone marrow MSCs (mesenchymal stem cells derived from bone marrow of adults) were purchased from Cyagen Biosciences Inc. (HUXMA-01001; Guangzhou, China) and cultured in MSCs specific growth medium (HUXMA-90011 and HUXMA-80011; Cyagen, China) at 37°C with 5% CO_2 according to manufacturer's instructions. MSCs used in our study have been authenticated by flow cytometry analysis and cell differentiation capacity tests provide by Cyagen Biosciences Inc. 3-5 passage MSCs were seeded onto PEG hydrogel at a density of 1×10^6 cells/mL. The cells used are Mycoplasm free.

METHOD DETAILS

Tissue analysis

To make sure the periodontitis was successfully induced, the bone level detection was performed using an eXplore Locus SP MicroCT scanner (GE Healthcare, USA) with proper X-ray energy (80 kV, 80 μA) and a voxel size of 9 μm. 2D and 3D images were acquired and analyzed by VGStudio MAX software.

To determine the PDL stiffness, fresh tissue samples were measured by nanoindenter (OPTICS11, Netherlands) with a microsphere indentation tip (diameter: 2.5 μm, stiffness: 0.49 N/m). The loading and unloading rate is 0.1mN/s and the maximum indentation force is 1mN. After the measurement, load-displacement curves were converted to load-indentation curves and fitted to the Hertz model as follows:

$$P = \frac{4}{3}\frac{E}{1-v^2}R^{1/2}h^{3/2} \quad \text{(Equation 1)}$$

where P is the load on the PDL, υ is the Poisson's ratio (the value is set to 0.5), R is the radius of the spherical tip, h is the indentation depth, and E is the Young's modulus of PDL to be determined. The Young's modulus measured here could reflect the stiffness of PDL.

For the SEM analyses, the fixed tissue specimens were dehydrated in 80%, 95%, and 100% ethanol. Then these specimens were grinded and polished at a suitable comparable position with sandpaper in an ascending grit fineness. To assess the periodontal tissue structures, 12% phosphoric acid was used to acid etch the polished surface. After washing ultrasonically by 5% sodium hypochlorite and dried, tissue specimens were coated with gold and palladium and detected with a FE-SEM system (GeminiSEM 500, ZEISS, Germany).

Histological examination of periodontitis

The fixed maxillae specimens were first decalcified in 0.5 M ethylenediaminetetraacetic acid (EDTA) for 4 weeks, with EDTA solution changed every 2 d. Specimens were then dehydrated in an increasing concentration (80%, 95%, and 100%) of ethanol before embedding in OCT (optimal cutting temperature compound, SAKURA, USA). After being sagittally sectioned (5 μm), tissue sections were baked at 55°C for 30 min. Tissue sections were stored at -80°C before further use. To further analyze the periodontal structure, hematoxylin-eosin (HE) was used to stain these tissue sections and images were taken by microscope (Olympus, Tokyo, Japan).

Preparation and characterization of PEG hydrogel substrate modified with RGD and TGF-β1 aptamer

15 μL 10% (wt%) of 8-arm PEG maleimide (8-arm-PEG-Mal, 10 kDa, JenKem Technology, USA) and 15 μL 5% (wt%) of 8-arm PEG thiol (8-arm-PEG-SH, 10 kDa, JenKem Technology, USA) were mixed and coverd with a hydrophilic slide to form a thin PEG hydrogel film. Meanwhile, 15 μL 5% (wt%) of 8-arm-PEG-Mal and 15 μL 3% (wt%) of 8-arm-PEG-SH were mixed to form another one. Besides, 10 nM rhodamine-labeled Arg-Gly-Asp (RGD, GCGYGRGDSSPG) and 5 nM FAM-labeled TGF-β1 aptamer (5′-SH- CGCTCGGCTTCACGAGATTCGTGTCGTTGTG TCCTGTACCCGCCTTGACCAGTCACTCTAGAGCATCCGGACTG-FAM-3′) were also added into the mixture to modify the hydrogel. Rhodamine and FAM were labeled respectively to help verify if the RGD and TGF-β1 aptamer were successfully modified onto the PEG hydrogel. After chemical crosslinking, the hydrogel was washed in PBS to remove unreacted molecules and observed using a fluorescence microscope (Olympus, Tokyo, Japan).

Fluorescence spectroscopy at 588 nm was used to determine the amount of the rhodamine-labeled RGD modified into the hydrogel film. The hydrogel films modified with RGD (without TGF-β1 aptamer) were put into residual incubation solution (*i.e.*, the initial incubation solution after immersing the hydrogel film) and centrifuged at 1500 rpm for 10 min. Both the supernatant with unreacted RGD and a blank solution (containing the same initial concentration of RGD during preparation) were diluted to the same volume in the incubation solution. The fluorescence values at 588 nm were measured to calculate the amount of grafted RGD.

After aptamers-patterned PEG hydrogel film was incubated in 200 μL DMEM with TGF-β1 protein (5 nM) overnight, the supernatant was then used to determine the levels of TGF-β1 using a human TGF-beta1 ELISA kit (Proteintech, IL, USA). All procedures were performed according to the manufacturer's instructions.

Hydrogel stiffness was also measured with the nanoindenter (OPTICS11, Netherlands) using the same method applied in measuring the PDL stiffness. After incubation in 200 μL DMEM *w/wo* TGF-β1 protein (5 nM) overnight, the stiffness of hydrogel films was measured at room temperature.

Analysis of TGF-β1 and integrin related gene expression

The gene-expression data of the PDL between patients with healthy periodontal ligament and patients with periodontitis were acquired from Gene Expression Omnibus (GEO; accession number GSE27993). The visualization of the results was realized by "pheatmap" packages in R software. We selected some TGF-β1 and integrin related genes for analysis.

MSCs viability

MSCs viability after seeding on PEG hydrogel was detected by live/dead assay. MSCs were incubated with live/dead fluorescent dyes (Invitrogen, USA) for about 15 min and then washed with PBS. Images were taken by a fluorescence microscope (Olympus, Tokyo, Japan) and MSCs viability was quantified using Image J software. Three replicates at least were measured for each group.

Analysis of TGF-β1 expression of MSCs on different stiffness substrates

After MSCs was cultured on different stiffness substrates without TGF-β1 for 12 h and 24 h, the supernatant was collected and used to determine the levels of TGF-β1 using a human TGF-beta1 ELISA kit (Proteintech, IL, USA). All procedures were performed according to the manufacturer's instructions.

Immunohistochemical staining

Immunohistochemical staining of tissue sections was performed using a streptavidin-HRP kit (CWBIO, China) according to the manufacturer's instructions. The primary antibody used here was anti-TGF-β1 antibody (1: 100; Abcam, USA).

Immunofluorescent staining

For immunofluorescent staining of rat specimens, sections were permeabilized with 0.5% Triton X-100 for 10 min and blocked in 10% goat serum for 30 min. Then the sections were incubated in primary antibodies of anti-integrin alpha V + beta 3 antibody (1: 200; GeneTex, USA) and anti-STRO-1 antibody (1: 25; Invitrogen, USA) at 4°C overnight and followed by the incubation of secondary antibodies for 2 h at room temperature. AlexaFluor 594 (1: 500; Cell Signaling Technology, USA) and AlexaFluor 488 (1: 500; Abcam, USA) were used to label anti-integrin alpha V + beta 3 and anti-STRO-1. DAPI (0.5 μg/ml; Cell Signaling Technology, USA) was dyed for visualizing cell nuclei.

For cell immunofluorescent staining, MSCs were fixed with 4% paraformaldehyde. The following procedures applied were the same with tissue section immunofluorescent staining mentioned before. The primary antibodies used here were as follows: anti-Runx2 antibody (1:100; Abcam, USA), anti-integrin alpha V + beta 3 antibody (1: 200; GeneTex, USA), anti-paxillin antibody (1: 100; Abcam, USA), anti-phospho-FAK antibody (1: 100; Abcam, USA), anti-YAP antibody (1: 200; Cell Signaling Technology, USA) and anti-lamin A/C antibody (1: 200; Cell Signaling Technology, USA). AlexaFluor 488, 594 and 647 (1: 1000; Cell Signaling Technology, USA) were used as secondary antibodies.

SiRNA transfection

MSCs were seeded onto a 6-well plate to be 70–90% confluent approximately 24 h before the transfection procedure. YAP siRNA and control siRNA were purchased from GenePharma (Shanghai, China). For cells in a well of 6-well plate, 4 μL Lipofectamine® 2000 reagent (Life Technologies, USA) was diluted with 200 μL Opti-MEM medium (Life Technologies, USA). Meanwhile, 8 μL YAP siRNA (sense: 5′-GACGACCAA UAGCUCAGAUTT-3′; 20 μM; GenePharma, China) or control siRNA (sense: 5′-UUCUUCGAACGUGUCACGUTT-3′; 20 μM; GenePharma, China) was diluted with 200 μL Opti-MEM medium. Then, the mixture of diluted Lipofectamine® 2000 reagent and the diluted siRNA was added to the MSCs and changed by fresh medium after incubation for 4 h. After culture in a fresh medium for 24 h, MSCs were harvested to evaluate the transfection efficiency in each group using real-time PCR and western blot analysis in parallel. The successfully transfected MSCs were used in the following experiments.

Inhibitior treatment by Verteporfin

In order to confirm their results of siRNA transfection, MSCs were treated with 10 μM verteporfin (Sigma, USA) for 24 h. Then MSCs were harvested in the following experiments. MSCs in control group and negative control group were incubated with no verteporfin and equal concentration of DMSO respectively.

Real-time PCR

Total RNA extraction, reverse transcription and quantitative real-time PCR were performed using TaKaRa MiniBEST Universal RNA Extraction Kit, PrimeScript RT Reagent Kit and SYBR Premix Ex Taq II Kit (TaKaRa Bio, Japan), respectively, according to the manufacturer's instructions. Primers used in our study are shown as follows: YAP-forward GAACAATGACGACCAATAGCTC, YAP-reverse TAGTCCACTGTCTGTACTC TCA, vinculin-forward CTGGAAAAGTTGGTGAACTCTG, vinculin-reverse CTTGATCAGTCATCTGCCCTAG, paxillin-forward CCTGACGAA AGAGAAGCCTAAG, paxillin-reverse CAGTTCATCCAAGAGACTCTCC, talin1-forward GACTTCAGACCCAAGTTATTGC, talin1-reverse CAGACAGGTGAGCTGATTGTAG, GAPDH-forward GGACCTGACCTGCCGTCTAG, and GAPDH-reverse TAGCCCAGGATGCCCTTGAG.

Three replicates at least for the real-time PCRs experiment. $2^{-\Delta\Delta Ct}$ method was used to calculate the messenger RNA expression.[15]

Western blot

To determine the protein level, western blot was performed according to the established protocol.[15] Primary antibodies used here were anti-YAP antibody, anti-vinculin antibody, anti-paxillin antibody, anti-FAK antibody, anti-phospho-FAK antibody and anti-GAPDH antibody (1: 1000; Cell Signaling Technology, USA). A chemiluminescence imaging system (Clinx, Shanghai, China) was used to visualize the bands.

Mathematical modeling analysis

Here, the mathematical model captured the regulatory processes observed in our experiments: (1) integrin β1-mediated YAP nuclear-cytoplasmic transport dynamics on different substrates of different stiffness or different levels of TGF-β; and (2) the combination of YAP and ITGB1 genes in the nucleus promotes integrin expression. The above two molecular processes form a mechanical autoregulation based on the combination of substrate stiffness and TGF-β level. Here, we used Gillespie stochastic simulation to simulate TGF-β-mediated mechanical

autoregulation in MSCs. The biochemical reactions, parameters (and the corresponding references) and description involved are shown in supplementary data (Tables S1 and S2). We calculated the distribution patterns under four conditions (e.g. TGF-β 1-/Soft, TGF-β 1+/Soft, TGF-β 1-/Stiff, TGF-β 1+/Stiff) for different parameters (e.g. r1). For example, the left table in Figure S11. Then, different distribution patterns were annotated with different markers (e.g. bimodal distribution represented by red circles), so that we could see how the distribution of cell adhesion changes (forward or reverse process) under each condition as the parameter value increases. For example, the right table in Figure S11. The final results are shown in Figure 5E.

Since integrins are key molecules in such stiffness mechanosensing, a key assumption is that the relationship between YAP nuclear in-rate and substrate stiffness is a Hill-type function, based on our previous study.[39] As shown in our experimental data, TGF-β can also increase the YAP n/c ratio. Therefore, for simplicity, we assumed that TGF-β can also promote the nuclear in-rate as a Hill-type function. The above Hill equation is $r_6 = K_N \frac{\alpha S+\beta T}{K_M+\alpha S+\beta T}$. Here, we use α and β to represent the regulatory strength of substrate stiffness and TGF-β on YAP nuclear in-rate. In our sensitivity analysis, we assume that stiffness and TGF-β have the different strength for integrin-mediated YAP nuclear entry, i.e., the coefficients of parameters S and T are α/β = 0.1-10 in the mathematical model. Note that according to our experimental data, the rate of YAP-mediated ITGB1 gene expression (here, the active state of ITGB1) is higher than that of the gene without YAP feedback (a basal state of ITGB1). In our model, we use the parameter k (from 1 to 100) to represent the increased amplification of the expression rate due to the state change of the gene (from the basal state to the active state).

However, there is currently no experimental basis for some of the relevant parameters. Therefore, we have adjusted all rate constants to perform a sensitivity analysis to ensure that the magnitude of the parameter values does not affect our conclusion. Similarly, for simplicity, the molecular number of YAP proteins is set to 1000, the same order of magnitude as Rho GEF according to ref. In fact, the main conclusions drawn from the model were not sensitive to the values chosen for the rate constants or the initial molecular number or rate constant (see details in the sensitivity analysis in the Document S1 of supplemental information). The initial numbers of molecular are: $G_{base} = 1$, $G_{active} = 0$, $N_{YAP}^{nuc} = 0$, $N_{YAP}^{cyto} = 1000 N_{integrin} = 0$. The simulation is allowed to run for 50000 time steps to ensure that the simulation has reached steady state before statistics are calculated. Each result is an average of 10 simulations. The codes were solved numerically using MATLAB (The Mathworks, Natick, Massachusetts).

QUANTIFICATION AND STATISTICAL ANALYSIS

All the experiment data in our study were collected at least three replicates per condition. Graphpad Prism 8 (8.0.1) or Origin (2020) was used to perform statistical analysis. Two-tailed Student's t-tests were used for the comparison between the two groups. One-way analysis of variance (ANOVA) with Tukey' post hoc test was performed for the comparison of multiple groups. Data were shown as the mean ± standard (SD). A p value of less than 0.05 was considered statistically significant. Significance was set at $P < 0.05$ (*), < 0.01 (**), or < 0.001 (***).